Submitted to Ultram Aussois Meeting 1988

X-RAY DETECTORS AND SPECTROMETERS

C. E. Lyman, D. B. Williams, and J. I. Goldstein
Materials Science and Engineering Department
Lehigh University
Bethlehem, PA 18015

X-ray emission spectroscopy using focused electron beams to excite the thin specimens provides elemental analysis with very high spatial resolution. The lithium-drifted silicon energy-dispersive spectrometer (EDS) is the only x-ray detector widely used in the analytical electron microscope (AEM). Future AEMs may employ an intrinsic germanium EDS detector to detect heavy element K-lines in addition to a Si(Li) detector optimized to detect the light elements such as 0, N, C, B, and possibly Be. The advantages of the wavelength-dispersive crystal spectrometer (WDS) complement those of EDS detectors and may be useful in an AEM optimized for high spatial resolution x-ray emission spectroscopy.

1. Introduction

X-rays may be generated within small volumes of a specimen from excitation by electrons, protons, or ions. Electron excitation of characteristic x-rays from very thin specimens provides the highest available spatial resolution of x-ray emission spectroscopy (XES) [1-2]. This review will cover only x-ray spectrometers and detectors compatible with the transmission electron microscope (TEM) or other electron optical instruments such as the scanning electron microscope (SEM) and the electron probe microanalyzer (EPMA). An x-ray spectrometer integrated with a TEM or a scanning transmission electron microscope (STEM) is an important form of the analytical electron microscope (AEM), and as such is the instrument of choice for providing x-ray emission spectrometry with the highest available spatial resolution.

The x-ray spectrometer based on a diffracting crystal of known d-value was devised by W. H. Bragg in 1913. In principle, this is the same device used today known as the wavelength-dispersive spectrometer (WDS). X-ray detector technology has progressed considerably in 75 years, from the ionization chamber that Bragg used on his original spectrometer to the semiconductor detectors used on some WDS units today. Note that in the WDS case the detector need only detect x-rays since the dispersion of their wavelengths or energies is accomplished by the analyzing crystal. The forerunner of the AEM, known as the electron microscope-microanalyzer (EMMA) developed by Duncumb [3] employed a WDS system to analyze thin specimens in a manner similar to that used by Castaing [4] to analyze bulk specimens. However, with the development of a semiconductor energy-dispersive spectrometer (EDS) capable of resolving characteristic peaks of first row transition elements [5], the EDS detector rapidly appeared on both SEMs [6] and TEMs [7], and the EMMA system relying on WDS fell into disuse. The EDS detector both detects x-rays and separates them according to energy. Moreover, whereas the WDS analyzing crystal must be placed at a precise angle with respect to a narrow beam of x-rays emanating from the specimen, the stationary EDS detector may be placed anywhere within the small space around the specimen in order to best subtend a large solid angle of emitted x-rays. The geometrical advantage in x-ray collection, about 10^2-10^3 greater than WDS, combined with the ability to simultaneously detect x-rays over a wide energy range without mechanical

motion, accounts for the present dominance of EDS systems for x-ray emission spectrometry in the electron microscope.

This paper reviews the current status of x-ray spectrometers and detectors used in analytical electron microscopy. Because of its importance, the ubiquitous EDS detector will be examined in the greatest detail. The paper describes the performance characteristics of various EDS and WDS systems now in use, discusses some of the difficulties encountered when incorporating these systems into electron microscopes, and suggests ways in which these x-ray spectrometers might be used in future applications.

2. Energy-Dispersive Spectrometers

The principles of operation and the performance characteristics of semiconductor EDS detectors will be illustrated by considering the liquid nitrogen-cooled lithium-drifted silicon detector. This was the first semiconductor EDS detector used in electron microscopy and continues to be the most widely used. With the availability of 300-400 kV microscopes, there are good reasons to consider using the intrinsic germanium detector in the AEM. In some applications liquid nitrogen cooling is either inconvenient or impossible. For these cases, it useful to consider detectors that may be cooled thermoelectrically or that operate satisfactorily at room temperature such as mercuric iodide detectors.

a) Si(Li) Detectors

Several previous reviews cover the principles of Si(Li) detectors in detail [8-13]. Only a brief summary is given here to describe the general characteristics of semiconductor EDS systems.

Principle of Operation. When an x-ray interacts with silicon, the energetic photon creates photoelectrons and Auger electrons which dissipate their energy by exciting Si valence electrons to the conduction band, potentially creating hundreds or thousands of electron-hole pairs [9]. The minimum energy to create an electron-hole pair is the band gap energy which for Si is 1.1 eV. Some of the incident x-ray energy is lost in the production of lattice vibrations, so the average energy ε required to create an electron-hole pair in Si is 3.8 eV at the typical working temperature of 100 K (liquid nitrogen). Thus, a Cu K_α x-ray of 8040 eV energy could potentially create 2115 electron-hole pairs. Clearly, the larger the number of electron-hole pairs created per incident x-ray, the smaller the statistical fluctuations in measured pulse heights and the better the energy resolution of the detector. In operation, the detector is negatively biased with about 500-1000 volts placed between the front and rear surfaces which separate the 2115 electrons and 2115 holes so they can be collected as a charge pulse that is proportional to the incident x-ray energy. This small charge (about 10^{-16} coulomb) is amplified in a low-noise, high-gain field effect transistor (FET) preamplifier near the detector crystal and further amplified and conditioned in a main amplifier located outside the LN_2 cryostat. The measured pulse representing a specific energy is then digitized and stored in a channel assigned to that energy in a multichannel analyzer (MCA).

Thermal energy can also excite electrons to the conduction band producing a dc leakage current which will add noise to the signal. At liquid nitrogen temperatures this contribution should be low for pure intrinsic silicon, however, all commercial high-purity Si contains acceptor impurities which increase the conductivity significantly. To compensate this p-type silicon, lithium is diffused into the detector from the backside to produce a large intrinsic region where the easily-ionized Li electrons combine with the impurity holes. Since the lithium distribution for complete compensation is obtained by diffusing and drifting Li into the Si under an electric field, this detector is often called a lithium-drifted silicon detector or Si(Li) detector. A thin gold contact layer is evaporated onto the front surface of the detector which is biased negatively. The backside of the detector is connected directly to the FET. Since the detector and FET must be kept cold to reduce noise, these components are usually sealed off from the ambient by a thin beryllium window (typically about 8 μm thick) which necessarily absorbs many of the x-rays less than 1 keV. A typical detector design is shown in **Figure 1**. The geometry of the detector is also important in

noise reduction, in particular, the detector is often fabricated with grooves on the backside to reduce surface leakage currents between electrodes.

The Detection Process. Incident x-rays passing through the Be window and the gold contact layer (typically 15 nm) are absorbed in either the 'dead' layer of uncompensated p-type Si or in the active layer of Li-compensated Si. An x-ray reaching the active volume of Li-compensated Si creates electron-hole pairs in a number proportional to its energy. The x-ray ionizes a silicon 1s (K-shell) electron and transfers all its energy, less the K-shell ionization energy, to this photoelectron which travels through the lattice creating more electron-hole pairs each time it is scattered until it comes to rest. The ionized Si atom returns to the ground state by emitting either an Auger electron or a Si K_α x-ray. The Auger electron also creates electron-hole pairs, while the x-ray deposits its energy by the same process as the incoming x-ray. Ideally, the entire energy of the incoming x-ray is converted into electron-hole pairs, and the incoming photon will be registered in the correct energy channel of the MCA.

Artifacts from the Detection Process. This detection process is not perfect and several spectral artifacts arise as other events take place. First, if the initial ionization of a Si atom takes place near the front surface of the active layer there is a probability that the emitted Si K_α x-ray can escape the detector. In this case, energy equal to the Si K_α x-ray (1.74 keV) will be lost from a strong x-ray peak at energy E but show up in a small peak, called the Si escape peak, at energy E - 1.74 keV. Its magnitude varies from about 1.8% of the parent peak at the phosphorus K-line to 0.01% at the zinc K-line [14]. Secondly, if the incoming x-ray excites a Si K_α x-ray in the thin 'dead' layer between the gold contact and the intrinsic region, this internally generated x-ray may travel into to the active layer and be measured as a Si x-ray. The resulting small Si peak in the spectrum is called the Si internal fluorescence peak. This peak may be present to an apparent level of 0.2 wt% Si even though there is no Si in the sample under examination. Thirdly, loss of electron-hole pairs may take place through recombination at defect traps near the edges of the detector and in the uncompensated p-type Si. This phenomenon, known as incomplete charge collection (ICC), robs certain x-ray counts of some of their energy and causes low energy tails to be displayed next to the peak. Current detector fabrication technology has reduced ICC effects on peak distortion to low levels for Si(Li) detectors.

Energy Resolution. The natural width of an x-ray line, about 2 eV, is broadened to about 150 eV by the detection process. The full-width-at-half-maximum (FWHM) energy resolution of an EDS x-ray detector may be expressed as the quadrature sum of an electronic noise contribution and an ionization statistics contribution:

$$FWHM^2 = \Delta E_n^2 + (2.35\sqrt{F\,\varepsilon\,E})^2 \ .$$

The electronic noise ΔE_n consists mainly of contributions from the FET itself (roughly 50%) and the detector leakage current (about 25%) [9]. Typical electronic noise contributions are less than 100 eV [15] and may be as low as 40-60 eV [16]. The second term is a function of the incoming x-ray energy E since the variation in the number of electron-hole pairs created in the detection of photon energy E will increase at higher photon energies due to the statistical nature of the ionization process. The Fano factor F is a material constant (~0.1 for Si) introduced to account for the fact that the observed variance in ionization is less than the theoretical statistical variance. The factor ε is the energy required to create an electron-hole pair (3.8 eV for Si). The distribution of pulses produced ideally should be Gaussian in a high quality detector. As the energy of the x-ray line increases, the width of this statistical distribution also increases and the measured energy resolution becomes poorer. Since the resolution varies with x-ray line energy, measurement of detector resolution must be made at the same peak energy. Thus, the IEEE standard for detector resolution measurement is the full-width-at-half-maximum (FWHM) of the Mn K_α peak generated by an Fe^{55} source. Typically Si(Li) detectors have a resolution of ~140-160 eV, although ~127 eV has been reported [16]. This value is very close to the theoretical limit (~120 eV) that would be obtained if electronic noise were completely eliminated. Detector resolution is also a function of detector area where larger detectors have poorer resolution because of higher electronic noise from the increased

capacitance. Figure 2 shows an x-ray spectrum taken with a 30 mm^2 windowless detector from a 100 nm thick sputtered Cr film [17].

Incomplete Charge Collection. Incomplete charge collection depends not only on the thickness of the uncompensated p-type Si layer beneath the front surface of the detector, but also upon the diffusion length of minority charge carriers (electrons) created within this layer. If these carriers do not reach the intrinsic region to be swept into the external circuit by the applied bias field, the carriers will be lost and the pulse measured will contribute to the low energy tail rather than to the main peak. Using Monte Carlo methods to model this effect Joy [18] predicted that the ICC effect is greater than 10% for all peaks below Na K. For x-rays of oxygen, nitrogen, and carbon the spectral distortions may be compounded by the fact that many of these low energy photons will not even reach the active intrinsic region of the detector. Joy also found that anomalous peak intensities and energy shifts for low energy peaks can be attributed to ICC effects. If the 'dead' layer were completely inactive, the detector would just have a lowered overall efficiency and some incident x-ray pulses would not be detected. This does not appear to be the case, rather all the pulses are detected and the ICC effect redistributes some the pulses to lower energies [19]. Measurements of the 'dead' layer thickness is difficult because of the complexities of the ICC phenomena. Estimates of effective 'dead' layer thicknesses in commercial Si(Li) detectors are typcially in the range 150-250 nm [18, 20-21].

Trapping of charge carriers and recombination can also occur at defects in the Si or in the thin oxide layer between the gold contact and the p-type Si [18]. Craven et al [22] have found that the effects of this trapping can be modified by external magnetic fields. Defects generated in these regions also have been implicated as a cause of the performance degradation often observed after exposure of the detector to a high flux of energetic electrons or x-rays. However, the details of these phenomena are not understood.

Count Rate Limitations. The penalty paid for energy-dispersed 'parallel' collection of the entire x-ray spectrum in a compact, non-moving device is a rather low count rate capability. Output counts usually approximate to input counts only up to about 2000 counts per second. The main amplifier must process each x-ray pulse sequentially; thus, a second pulse entering the detector before processing of an earlier pulse is complete would result in the display of a pulse that is the sum of the two pulse energies. Pulse processing times may be reduced only at the expense of achievable energy resolution. Processing and shaping times can range from about 5-100 μs, depending on the particular amplifier circuit used. To eliminate spurious sum peaks caused by coincident and near-coincident pulses, a fast amplifier with an extremely short processing time (and consequently very poor energy resolution) is used to identify coincidence events so they can be eliminated from the spectrum. The time during which the detector is handling coincident pulses is called 'dead time' since it cannot be used to build up the measured spectrum. Dead times of 20-30% should be used to obtain high quality data, while the greatest throughput of counts usually occurs near 70% dead time.

Detection Efficiency. Collection efficiency is a most important detector parameter when the highest spatial resolution is sought along with the least possible electron beam damage to the specimen. Overall efficiency is defined as the x-ray count rate per electron incident on the specimen, and this is dependent on the effective solid angle that the sensitive area of the detector subtends with respect to the analysis area on the specimen. This solid angle may be increased by increasing the detector area (sacrificing some energy resolution) and by positioning the detector as close to the specimen as possible. Collection solid angles of about 0.1 steradian have been achieved for detectors with Be windows but higher values are possible with special detector designs.

X-rays in the energy range 5-20 keV are detected with nearly 100% efficiency in a typical Si(Li) detector. Below 5 keV x-rays entering the detector are absorbed in the Be window, the gold contact layer, and the silicon dead layer. The Be window causes the most serious losses; for example, an 8 μm Be window will reduce the intensity of a 1 keV x-ray to about 50% of its original value. Clearly, the use of alternative light-element window materials, or removal of the

window altogether, will improve detection of the light elements dramatically (see ultra-thin window and windowless detectors below).

Above 20 keV x-rays have enough energy to pass through the detector without being absorbed or measured. The thickness of most Si(Li) detectors is 3 mm which provides 100% efficiency out to nearly 20 keV. For 100 kV electron microscopes, this thickness is adequate since x-rays of energy higher than 20 keV are not strongly excited. However, this situation forces the analyst to use a combination of K-, L-, and M-lines to cover all the elements in the periodic table. For some analyses it would be helpful to use K-lines instead of L- and M-lines for the heavier elements (see intrinsic Ge detectors below).

Ultra-thin Window Detectors. Window materials that are less absorbing than Be are often constructed of a thin polymer membrane such as parylene which is coated with a thin film of aluminum to prevent the transmission of visible light from cathodoluminescent samples which would also generate electron-hole pairs in the Si(Li) crystal. The best ultra-thin window (UTW) systems can detect boron in samples containing significant amounts of the element. Unfortunately, the conventional UTW is rather delicate and not able to withstand atmospheric pressure. This type of detector must be withdrawn behind a vacuum isolation valve whenever the column is vented to atmosphere. The extra valving required makes the UTW-EDS design more complex and sometimes forces the detector to be positioned further from the specimen than a conventional Be window detector, causing a loss of collection angle. Recent commercial developments have resulted in proprietary UTW materials capable of withstanding atmospheric pressure while still transmitting boron K_α x-rays [23].

Windowless Detectors. Collection of low energy x-rays will be most efficient if the window is completely removed. Windowless systems were tried soon after Si(Li) detectors were first employed on electron microscopes [24], but microscope vacuums were relatively poor and the detector surface contaminated rapidly. The windowless design is only viable in an ultra-high vacuum (UHV) AEM where great care is taken to eliminate hydrocarbons and water vapor. Nevertheless, over a period of time, even in an UHV environment, ice buildup will eventually compromise the detector efficiency at the low end of the spectrum. This ice layer can be removed by warming the detector to a temperature high enough to sublime off the ice. By comparing the ratio of the Ni-L line to the Ni-K_α line before and after such a warmup, the ice layer on the surface of a windowless detector after one year in UHV was found to be about 3 μm thick (see **Figure 3**). Automatic in-situ heating devices now make this warmup process routine [17]. Evidence for ice layers up to 12 μm in sealed Be window detectors has been found by other methods [25]. With a windowless system and special amplification circuitry, Be K_α x-rays from solid Be have been detected [26].

A comparison of x-ray transmission versus incoming x-ray energy for various detector window materials is shown in **Figure 4**. Note that the efficiency of an ultra-thin window detector is nearly as good as that of a windowless detector. Since one of the difficulties in using the conventional UTW is its extreme fragility, the advantage of the Kevex Quantum UTW, that may be cycled to atmospheric pressure during a specimen change, is clear.

b) Intrinsic Germanium Detectors

Since it is possible to manufacture higher purity Ge than Si, a large intrinsic region can be produced in this material without the need for Li compensation. A detector made of high purity Ge (HPGe) has several advantages. The most obvious advantage is that Ge will absorb more high energy x-rays for the same detector thickness than Si as shown in **Figure 5**. Thus, the K-lines of heavy elements that are generated in AEMs operating at 300-400 kV can be detected. **Figure 6** shows the well-resolved K_α-lines of lead from a lead glass specimen [27]. Although in this case the intensities are low, the use of K-lines for heavier elements has important consequences for microanalysis. There are cases where Cliff-Lorimer sensitivity factors (k-factors) cannot be conveniently measured from standards and must be calculated. The error in the calculation of k-factors for K-lines is typically about one-third that for L-lines [28].

There are even more fundamental reasons for the use of intrinsic germanium (IG) detectors. Since the average energy to create an electron-hole pair in Ge is 2.9 eV versus 3.8 eV in Si, statistical peak broadening or dispersion is less for Ge detectors. This means that IG detectors should have a better ultimate energy resolution than Si(Li) detectors. The best value reported for an IG detector is 118 eV [29] versus 127 eV for a Si(Li) detector. Because there is never any danger of losing detector performance by destroying the Li-drifted region, the IG detector is more robust and may be warmed to room temperature repeatedly. Until recently IG detectors have been plagued by severe incomplete charge collection which caused intense low energy tails on peaks just above the germanium L absorption edges [30-31]. By improvement in fabrication technology, especially by limiting the growth of oxide between the crystal and the gold contact, the ICC problem has been greatly reduced [29] as shown in **Figure 7**. Recent IG detectors, with appropriate amplifiers, have excellent low energy performance as demonstrated by the detection of a well-resolved boron peak (see **Figure 8**).

There are some difficulties in using IG detectors to detect K-lines. The most serious problem is the order of magnitude decrease in ionization cross section for K-lines at 200-400 kV [27]. Also, a slight problem of spectrum interpretation exists when using IG detectors on intermediate voltage AEMs. There will be many more escape peaks to keep track of, but this should not be a serious barrier to using IGs in practice because many MCAs can identify escape peaks and automatically add their intensities to the parent peaks. Indeed, it is reasonable to propose that many intermediate voltage AEMs be equipped with two detectors, an IG for heavy elements and a UTW Si(Li) optimized for light element detection.

c) Mercuric Iodide Detectors

Perhaps the major inconvenience associated with EDS detectors is the need for continuous liquid nitrogen cooling. Thermoelectric cooling has been introduced for certain Si(Li) detectors, but a compact room temperature detector is still not a commercial product. Development of room temperature mercuric iodide (HgI_2) detectors and associated near-room temperature ultra-low noise preamplifiers has been underway for several years [32]. These detectors have now attained a resolution of 225 eV at 5.9 keV [33]. This room temperature performance is possible because the relatively large 2.2 eV band gap of HgI_2 (vs. 1.1 eV for Si) gives the material a high resistivity, and thus a low leakage current at room temperature. The corollary to this, however, is that the consequent higher energy required to create an electron-hole pair in HgI_2 (4.2 eV) limits the ultimate energy resolution to values considerably higher than those of Si(Li) detectors. To obtain the best possible energy resolution, these detectors also require liquid nitrogen or thermoelectric cooling. A serious drawback of these systems for use as EDS detectors in AEMs is the very small detector area, typically 5 mm^2 compared to 10-30 mm^2 for Si(Li) and IG detectors. Another problem is that for operation in ultra-high vacuum environments the detector material must be encapsulated in a polymer or other material to prevent sublimation into the vacuum [34]. This type of detector, however, may find use in certain applications where energy resolution and detector area are not as important as room temperature operation, such as for the detector of a WDS system.

d) Comparison of Semiconductor Detector Materials.

A comparison of the properties of these three types of semiconductor detector materials is shown in **Table 1.** Note that the better the ultimate energy resolution of a particular detector, the greater is the need to cool the detector. The iG detector exhibits the best energy resolution since the energy to create electron-hole pairs is the least of the three; however, since Ge has the smallest band gap, leakage currents due to its lower resistivity will be more of a problem unless the detector material itself is cooled to low temperatures. When the detector itself is carefully manufactured and appropriately cooled, it is then the noise characteristics of the FET preamplifier (also cooled) that most seriously limit the attainable energy resolution of IG detectors. The very successful Si(Li) detector appears to be a good compromise.

e) Pulse Processing Electronics.

All three detectors described above usually employ similar pulse processing and display electronics. Completely electronic energy dispersion requires that the pulse processing electronics maintain good energy resolution across the spectrum without peak shift or distortion, even at high counting rates. To accomplish this all electronic components beyond the detector crystal must have low noise characteristics and must employ some means of handling pulses that arrive in rapid succession.

Conventional Pulse Processors. After the energy of an x-ray photon is converted to electron-hole pairs which are swept into the external circuit by the bias voltage, the charge-sensitive FET preamplifier registers this charge as a step in a staircase of increasing charge. When no more charge can be stored, counting is interrupted, and a light-emitting diode discharges the accumulated charge to reset the amplifier. The main amplifier, commonly called a pulse processor, converts the staircase waveform to a sequence of individual pulses which are passed to an analog-to-digital converter (ADC). The digital pulses of various heights (energies) are stored in a computer or MCA and displayed as a number of pulses versus pulse energy of channel number, i.e., the x-ray spectrum.

Improvements in these components have generally involved noise reduction in the FET and schemes to reject pulses that enter the detector too close together in time to be properly resolved as separate pulses. The latter feature, known as pulse-pileup rejection, governs the maximum count rate capability of the system. Generally, two amplifier channels are used. The slow channel uses a long time constant to process each pulse with a high signal-to-noise ratio, and thus provides good energy resolution for the peaks building up in the spectrum. If a second pulse reaches the slow amplifier before the first pulse is completely processed, a sum pulse would be stored in the spectrum. This undesirable effect may be avoided by discarding both pulses and assuming that the time associated with this process is part of the system 'dead' time. To sense when pulses arrive too close together to be resolved, a fast amplifier channel of short time constant but poor energy resolution is used. Most of the development in recent years has involved improvements in pulse-pileup rejection at very low energies where it is difficult to discriminate a true low energy pulse from the electronic noise peak [10].

Kandiah-Harwell Pulse Processor. Kandiah [35] designed an amplifier based on the time-variant pulse processing approach. In this system a recognition channel senses the arrival of a pulse and sets long time constants to provide a very high signal-to-noise ratio and thus high energy resolution during pulse amplification. After the ADC has digitized the pulse, the time constants are switched to shorter times to rapidly restore the amplifier to the baseline level. The processor is then ready to accept a second pulse much sooner than it would be with the conventional system described above. This device can double the maximum throughput rate and modifications to this processor have been used to improve pulse pileup rejection for the low energy x-rays obtained with UTW and windowless detectors [12]. Although it is still wise to use low count rates to obtain the best spectra for very low energy x-rays [13].

High speed beam blanking may be used to obtain effective pileup rejection at even higher count rates [36]. Electrostatic switching of the electron beam to and from a position on an aperture at megahertz frequencies can allow recording of x-ray pulses at about three times the normal rate [37]. For field-emission AEMs generating electron beams of extremely high current density, this method has the advantage of reducing electron beam damage at the same time.

f) EDS Detector-Microscope Interface

Detector Performance. All guaranteed detector energy resolution specifications are measured by exciting the detector with Mn K_α x-rays from an Fe^{55} source when the detector is removed from the microscope. The energy resolution performance when the EDS system is operated as part of a functioning AEM is generally worse than that measured on the bench. In addition, the effects of microphonics, ground loops, detector window contamination, spurious x-rays generated remotely from the beam, high fluxes of x-rays and electrons, electromagnetic

interference, and amplifier saturation may also hamper x-ray microanalysis in an operating AEM [38]. Rather than merely attaching an EDS detector to a TEM in any fashion that will fit into the objective lens, considerably better AEM x-ray performance would be obtained if the entire microscope were designed around the optimum EDS detector-specimen arrangement [39].

Solid Angle of X-ray Collection. The minimum mass fraction (MMF) of one element detectable in another decreases with increasing peak-to-background ratio (P/B) and increasing peak intensity (P). To increase the number of x-ray counts (P) detected from a specimen, either the current in the electron probe must be increased, usually at the expense of analytical spatial resolution [40], or the collection angle of the x-ray detector must be increased. Since increasing the current density in the electron probe will also increase electron beam damage to the specimen, increasing the x-ray collection angle is clearly preferred. Most electron microscopes are designed primarily for high performance in imaging and thus have polepiece configurations with narrow gaps to provide the highest image resolution. It is interesting to consider whether an increased x-ray signal may be obtained by enlarging the polepiece gap and placing the x-ray detector closer to the specimen even though the probe current onto the specimen will decrease due to the larger spherical aberration coefficient.

The peak-to-background ratio expected from a thin specimen in an AEM increases with x-ray take-off angle [41]. As the collection angle is increased to high values, the take-off angle becomes less well-defined making quantitative analysis employing an absorption correction less accurate. This problem can be avoided if the detector is designed to retract from specimen along a line-of-sight to the specimen. With this configuration sensitive qualitative analysis can be obtained when the detector is close to the specimen and quantitative analysis can be obtained when the detector is slightly retracted so as to better define the take-off angle.

3. Wavelength-Dispersive Spectrometers

Wavelength-dispersive x-ray spectrometers (WDSs) play an important role in x-ray fluorescence measurements at a spatial resolution of a few millimeters and in the electron probe microanalyzer (EPMA) at a spatial resolution of a few micrometers [9]. The advantages of WDS over EDS are: a) better energy resolution to unravel the pathological peak overlaps that plague EDS, b) better peak-to-background capability to detect smaller amounts of elements, and c) better detection of light elements by crystal diffraction rather than solely through a dependence upon electronics as in the EDS case. Generally, WDS systems have not been applied to AEMs for high spatial resolution analysis because of their traditionally low x-ray collection efficiency compared to that of EDS detectors. The advantages of the WDS, however, may make it an attractive complement to the EDS in future AEMs. Only WDS designs compact enough to be placed inside an AEM specimen stage, for improved collection efficiency, are reviewed here.

a) Spectrometer Designs

Focusing Crystal Spectrometers. Most WDS systems used in the EPMA rely upon fully focusing crystal x-ray optics [42,43] rather than semi-focusing optics [44,45]. This is largely because most EPMAs are designed to have considerable room around the specimen to locate large, and often complex, x-ray optical devices for optimal spectral resolution. The large dimensions of these spectrometers also simplify the fabrication of precisely bent (Johann optics) or bent and ground (Johansson optics) analyzing crystals. The large focusing circles (10-20 cm radius) of these WDS units are largely responsible for their small solid angle of x-ray collection, typically 0.0001-0.001 steradians. To increase the x-ray collection efficiency, a double-focusing effect may be obtained by bending the crystal planes to a radius 2R in two directions or doubly bending to 2R and grinding to a spherical shape of radius R on the inner surface [46]. For the latter configuration of a doubly-bent Johansson crystal, the diverging x-ray beam from the specimen makes the appropriate Bragg angle with the crystal over its entire surface. Fabrication of these special crystals out of germanium has been demonstrated [47] as shown in **Figure 9**. By using a crystal

of this type, and at the same time reducing the size of the focusing circle, a WDS of high efficiency could be constructed for use in an AEM [48].

Synthetic Multilayer Analyzing Crystals. Conventional analyzing crystals include several natural crystals (LiF, quartz, etc.) of various d-values to disperse the various x-ray wavelengths (energies) according to Bragg's Law: $n\lambda = 2d\sin\theta$. For the low energy x-rays of light elements, fragile soap film 'crystals' of large d-value are traditionally used. With the advent of microfabrication technology, several layered synthetic microstructures have been developed to diffract and disperse the low energy x-rays of the light elements such as B, C, N, and O [49]. These devices consist of alternating layers of a heavy metal and a light element, e.g., W-Si. By optimizing the heavy metal layer spacing in these structures, diffracted intensities can be 2-3 times higher for oxygen x-rays than when using lead stearate soap film 'crystals', however, the energy resolution obtained is somewhat poorer [50,51].

Other Spectrometer Designs. Another compact spectrometer that has been used is one in which a flexible crystal such as mica is mechanically bent such that the focusing circle radius varies as a function of θ [52]. This system has the advantage that a flexible synthetic multilayer structure could be deposited on the surface to analyze the light elements at the same time. For the very lightest elements, such as Be and B, a simple grating spectrometer operating at a glancing angle may be useful in an AEM [53].

b) Detectors

An x-ray detector for a small UHV-compatible WDS unit to be used inside a modern AEM must be efficient, have modest energy resolution (<1000 eV) at room temperature, and preferably should be bakable to at least 100 C. Traditional sealed gas proportional detectors provide considerable gas gain and might be made compatible with UHV by using an x-ray window similar to that of the Kevex 'Quantum' detector. But the small size required for the AEM may restrict the achievable detector voltage (and gas gain), and the device may not be bakable. Modern construction technologies could shrink the scintillation-photomultiplier detector to a useable size, but absorption of soft x-rays by the casing of the phosphor have usually limited scintillation counters to energies > 4 keV [54]. Silicon detectors usually are not operated at room temperature as shown in **Table 1**. However, ion-implanted Si detectors have been developed with 1.3 keV energy resolution for 14.4 keV at room temperature [55]. This resolution should be adequate for separating overlapping orders of diffraction n. For the inside of an AEM, a properly encapsulated HgI_2 detector may also be possible since it is small, efficient, and has excellent energy resolution at room temperature.

4. Conclusion

Focused electron beams offer the best opportunity for high spatial resolution analysis using x-ray emission spectroscopy. Currently, the Si(Li) EDS system is by far the most widely used spectrometer on analytical electron microscopes, however, future AEMs may employ both an intrinsic Ge detector for detection of heavy element K-lines and a Si(Li) detector optimized for detection of light elements. The advantages of the WDS system make it an attractive additional complement to the Si(Li) detector on an AEM. Design of these spectrometers and the microscope together should result in an AEM optimized primarily for high spatial resolution x-ray emission spectroscopy.

Acknowledgements

The authors thank J.R. Michael for the use of his unpublished data and the Bethlehem Steel Corporation for use of the VG HB-501 STEM. B. G. Lowe made many helpful suggestions on the manuscript and provided some unpublished data. The authors wish to acknowledge the support of their work by DOE through DE-FG02-86ER45269 and by NASA through NAG 9-45.

References

[1] D.C. Joy, A. D. Romig, and J. I. Goldstein (Eds.), Principles of Analytical Electron Microscopy (Plenum, New York, 1986).
[2] D. B. Williams, Practical Analytical Electron Microscopy in Materials Science (Philips Electron Optics Publishing) Mahwah, New Jersey, 1984.
[3] P. Duncumb, in: The Electron Microprobe, Eds. T. D. McKinley, K. F. J. Heinrich, and D. B. Wittry (Wiley , New York, 1986) p.490.
[4] R. Castaing, Ph. D. thesis, University of Paris, 1951.
[5] E. Elad and M. Nakamura, Nucl. Instrum. Meth. 9 (1966) 161.
[6] R. Fitzgerald, K. Keil, and K. F. J. Heinrich, Science 159 (168) 528.
[7] S. L. Bender and R. H. Duff, STP 485, (ASTM, Philadelphia, 1971) p. 180.
[8] D. R. Beaman and J. A. Isasi, STP 506, (ASTM, Philadelphia, 1972).
[9] S. J. B. Reed, Electron Microprobe Analysis, (Cambridge University Press, 1975).
[10] C. E. Fiori and D. E. Newbury, in: Scanning Electron Microscopy, 1978, Ed. O. Johari, vol. I (SEM, Inc, O'Hare, Illinois, 1978) p. 401.
[11] R. W. Fink, in: NBS Special Publ. 604, Ed. K. F. J. Heinrich, D. E. Newbury, R. L. Myklebust, and C. E. Fiori, (U. S. Gov. Printing Off., Washington, DC, 1981), p. 5.
[12] P. J. Statham, J. Microscopy 123 (1981) 1.
[13] P. J. Statham, J. Microscopy 130 (1983) 165.
[14] R. Woldseth, X-ray Energy Spectrometry (Kevex Corp., Foster City, California, 1973).
[15] C. E. Cox and K. Kandiah, Proc. 6th Intl. Symp. Noise in Physical Syst. (National Bureau of Standards, 1981).
[16] B. G. Lowe, 1988, private communication.
[17] D. B. Williams and E. B. Steel, Analytical Electron Microscopy -- 1987 (San Francisco Press, 1987) p.228.
[18] D. C. Joy, Microbeam Analysis -- 1985 (San Francisco Press, 1985) p. 342.
[19] A. J. Craven, P. R. Adam, and R. Howe, EMAG-85, Inst. Phys. Conf. Ser. No. 78 (Adam Hilger, 1985) p. 189.
[20] J. Heckel and W. Scholz, X-ray Spectrom. 16 (1987) 181.
[21] J. L. Campbell, A. Perujo, and B. M. Millman, X-ray Spectrom. 16 (1987) 195.
[22] A. J. Craven, these proceedings.
[23] G. Aden and D. Isaacs, Research and Development 29 (No. 8 1987), 85.
[24] J. M. Jaklevic and F. S. Goulding, IEEE Trans. Nucl. Sci., NS-18 (1971) 187.
[25] D. D. Cohen, X-ray Spectrom. 16 (1987) 237.
[26] P. J. Statham, Proc. of ANRT meeting on Microanalysis and Scanning Electron Microscopy, Paris, 1985.
[27] E. B. Steel, Microbeam Analysis -- 1986, (Eds.) A. D. Romig and W. F. Chambers (San Francisco Press, 1986) p. 439.
[28] J. E. Wood, D. B. Williams, and J. I. Goldstein, J. Microscopy 133 (1984) 225.
[29] C. E. Cox, B. G. Lowe, and R. A. Sareen, IEEE Trans., in press.
[30] J. Llacer, E. E. Haller, and R. C. Cordi, IEE Trans., Nucl. Sci. vol. NS-24 (1977) 53.
[31] N. C. Barbi and D. B. Lister, NBS Special Publication No. 604 (1981) p. 35.
[32] A. J. Dabrowski, M. Singh, G. G. Huth, and J. S. Iwanczyk, NBS Special Publication No. 604 (1981) p. 45.
[33] W. K. Warburton and J. S. Iwanczyk, Scanning Microscopy Suppl 1 (Scann. Micros, Intl., Chicago, Illinois, 1987) p. 135.

[34] W. K. Warburton, 1987, private communication.
[35] K. Kandiah, A. J. Smith, and G. White, IEEE Trans. Nucl. Sci., NS-22 (1975).
[36] P. J. Statham, X-ray Spectrom. 6 (1977) 94.
[37] J. M. Jaklevic, E. S. Goulding, and D. A. Landis, IEEE Trans. Nucl. Sci. NS-19 (1972) 392.
[38] D. B. Williams, J. I. Goldstein, and C. E. Fiori, in: Principles of Analytical Electron Microscopy, (Eds.) D. C. Joy, A. D. Romig, and J. I. Goldstein (Plenum, New York, 1986) 123.
[39] D. B. Williams, Microbeam Analysis -- 1986, (San Francisco Press, 1986) p. 443.
[40] C.E. Lyman and J. R. Michael, Analytical Electron Microscopy -- 1984, Ed. D. C. Joy, (San Francisco Press, 1986), 231.
[41] N. J. Zaluzec, in: Introduction to Analytical Electron Microscopy, Eds. J. J. Hren, J. I. Goldstein, and D. C. Joy, (Plenum, New York, 1979), p. 121.
[42] H. H. Johann, Z. Physik 69 (1931) 185.
[43] T. Johansson, Z. Physik 82 (1933) 507.
[44] J. V. P. Long and V. E. Cosslett, in: X-ray Microscopy and Microradiaography, Eds. V. E. Cosslett, et al. (Academic Press, New York, 1957), p. 435.
[45] E. F. Priestley in: Proc 6th Intl. Conf. X-ray Optics and Microanal., Eds. G. Sinoda, K. Kohrn, and T. Ichinokawa (University of Tokyo Press, 1972) p. 345.
[46] D. B. Wittry, U. S. Patent No. 4,599,741 (1986).
[47] D. M. Goliganin and D. B. Wittry, in: Microbeam Analysis -- 1987, Ed. R. H. Geiss (San Francisco Press, 1987) p. 51.
[48] J. I. Goldstein, C. E. Lyman, and D. B. Williams, these proceedings.
[49] J. A. Nicolosi, J. P. Groven, D. Merlo, and R. Jenkins, Optical Engineering 25 (1986) 964.
[50] T. Arai and R. W. Ryon, in: Adv X-ray Analysis, Vol.28, Eds. Barrett, Predecki, and Leyden, (Plenum, New York, 1985) p. 137.
[51] K. Kawabe, A. Kato, T. Tomita, and S. Tagata, in: Proc 11th Intl. Cong. on Electron Microscopy, Kyoto, 1986, p.569.
[52] H. A. Elion and R. E. Ogilvie, Rev. Sci. Inst. 33 (1962) 753.
[53] G. Date, Y. Nakajima, Y. Ohmori, T. Shiraiwa, and N. Fujino, in: Proc. 6th Intl. Conf. X-ray Optics and Microanalysis, Eds. G. Shinoda, K. Kohrn, and T. Ichinokawa, (Univ. of Tokyo Press, 1972) p. 333.
[54] R. Jenkins and J. L. De Vries, Practical X-ray Spectrometry, (Springer-Verlag, New York, 1967).
[55] P. Burger, M. O. Lampert, R. Henck, and J. Kemmer, IEEE Trans. Nucl. Sci., NS-31, (1984) 334.
[56] R. G. Musket, NBS Special Publication 604 (1981), p. 97.
[57] B. G. Lowe, 1988, private communication.
[58] Kevex commercial literature.
[59] C. E. Cox, 1988, private communication.

Table 1: Comparison of Semiconductor X-ray Detector Materials

Characteristic	Intrinsic Ge	Lithium-drifted Si	HgI_2
Energy resolution			
Typical	140 eV	150 eV	250 eV
Current best	118 [29]	127 [16]	225 [33]
Energy required to form electron-hole pairs	2.9 eV [11] (77 K)	3.8 eV [8] (77 K)	4.2 eV [32] (300 K)
Band gap energy	0.67 eV	1.1 eV	2.1 eV
Cooling required	LN_2 or thermoelectric	LN_2 or thermoelectric	Thermoelectric or none
Typical detector active area	10-30 mm^2	10-30 mm^2	5 mm^2

Figure Captions

Fig.1. Cross-section of a groove-type Si(Li) detector crystal (from Statham [12], courtesy J. Microscopy).

Fig.2. Spectrum of a thin sputtered Cr film [17] from a windowless Si(Li) detector. The extra peaks are from the noise peak (0 eV), carbon (280 eV) from the support film, and copper (8.04 keV) from the support grid (courtesy J.R. Michael).

Fig.3. Carbon K, oxygen K, and nickel L peaks before detector warmup (solid curve) and after warming detector crystal to about 70-80°C (dotted curve). The nickel K-lines were of equal intensity for each curve. This change in absorption characteristics corresponds to an ice layer 3μm thick built up over a period of one year (courtesy J.R. Michael).

Fig.4. Low energy efficiency calculated for a windowless detector (curve a) [56], a conventional ultra-thin window detector (curve b) [57], the Kevex Quantum window (curve c) [58], and a conventional Be window detector (curve d) [58]. Absorption edges have been omitted for clarity.

Fig.5. High energy efficiency calculated for Si(Li) and intrinsic Ge detectors. Detector thickness assumed to be 3 mm in both cases [59].

Fig.6. Lead $K_{\alpha 1}$ and $K_{\alpha 2}$ lines from lead silicate glass analyzed in a 200 kV AEM with an intrinsic Ge detector [27] (courtesy San Francisco Press).

Fig.7. Low energy peaks detected with an intrinsic Ge detector showing a low level of incomplete charge collection [29].

Fig.8. Boron K_{α} peak collected with an intrinsic Ge detector (courtesy Link Systems).

Fig.9. Schematic diagram of a doubly-bent diffracting crystal for a wavelength-dispersive spectrometer [46].

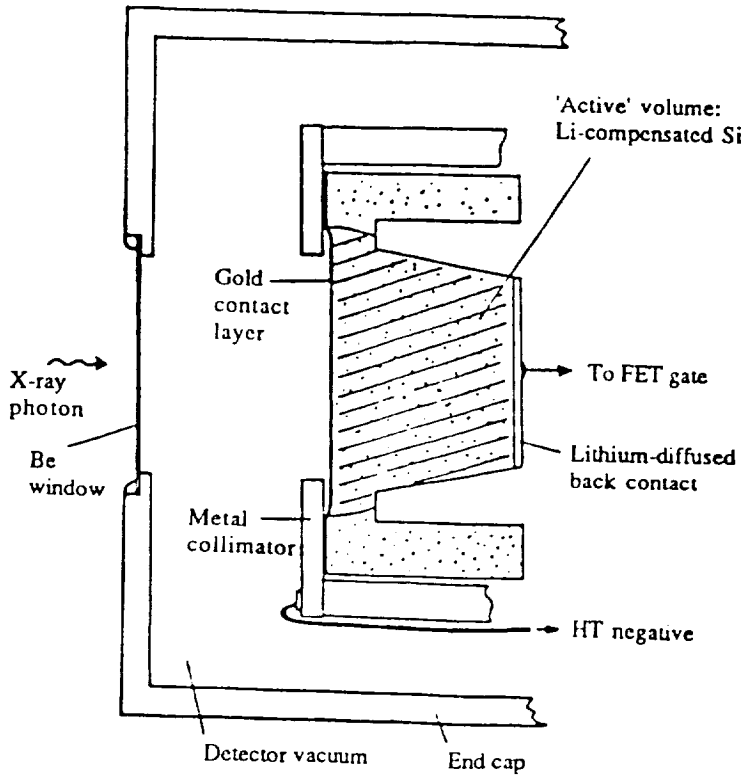

Fig.1. Cross-section of a groove-type Si(Li) detector crystal (from Statham [12], courtesy J. Microscopy).

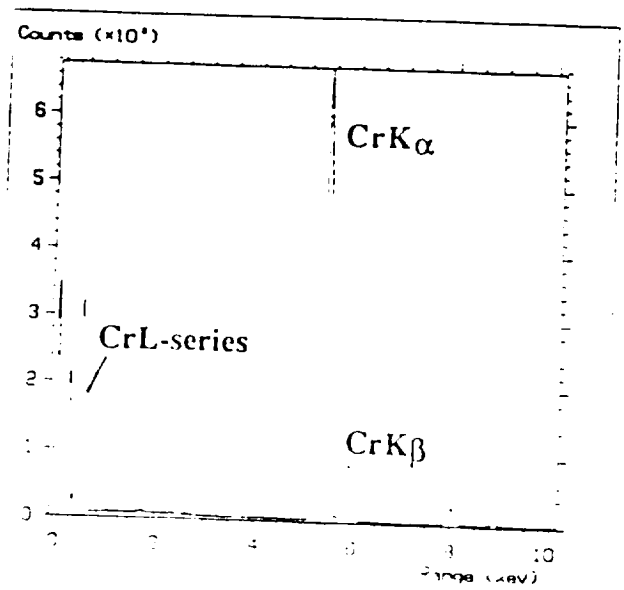

Fig.2. Spectrum of a thin sputtered Cr film [17] from a windowless Si(Li) detector. The extra peaks are from the noise peak (0 eV), carbon (280 eV) from the support film, and copper (8.04 keV) from the support grid (courtesy J.R. Michael).

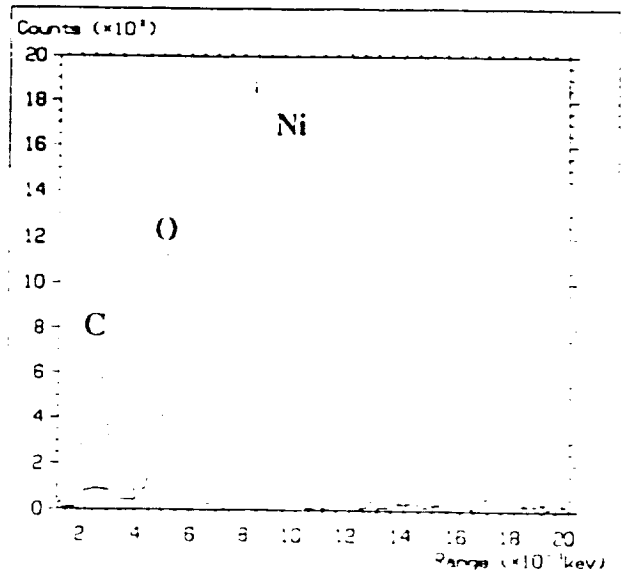

Fig.3. Carbon K, oxygen K, and nickel L peaks before detector warmup (solid curve) and after warming detector crystal to about 70-80°C (dotted curve). The nickel K-lines were of equal intensity for each curve. This change in absorption characteristics corresponds to an ice layer 3μm thick built up over a period of one year (courtesy J.R. Michael).

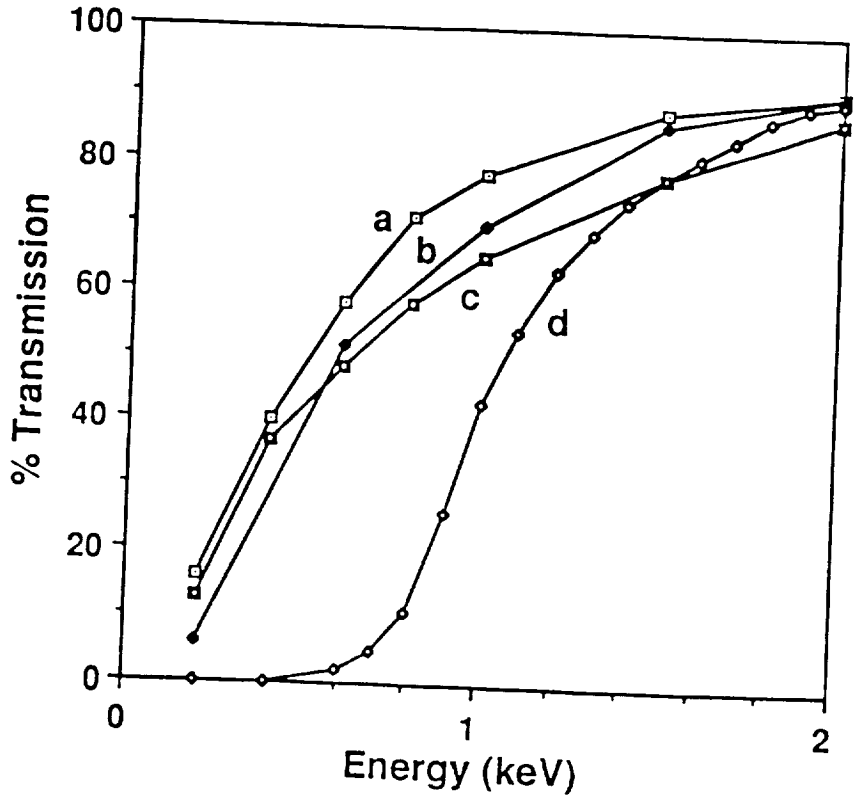

Fig.4. Low energy efficiency calculated for a windowless detector (curve a) [56], a conventional ultra-thin window detector (curve b) [57], the Kevex Quantum window (curve c) [58], and a conventional Be window detector (curve d) [58]. Absorption edges have been omited for clarity.

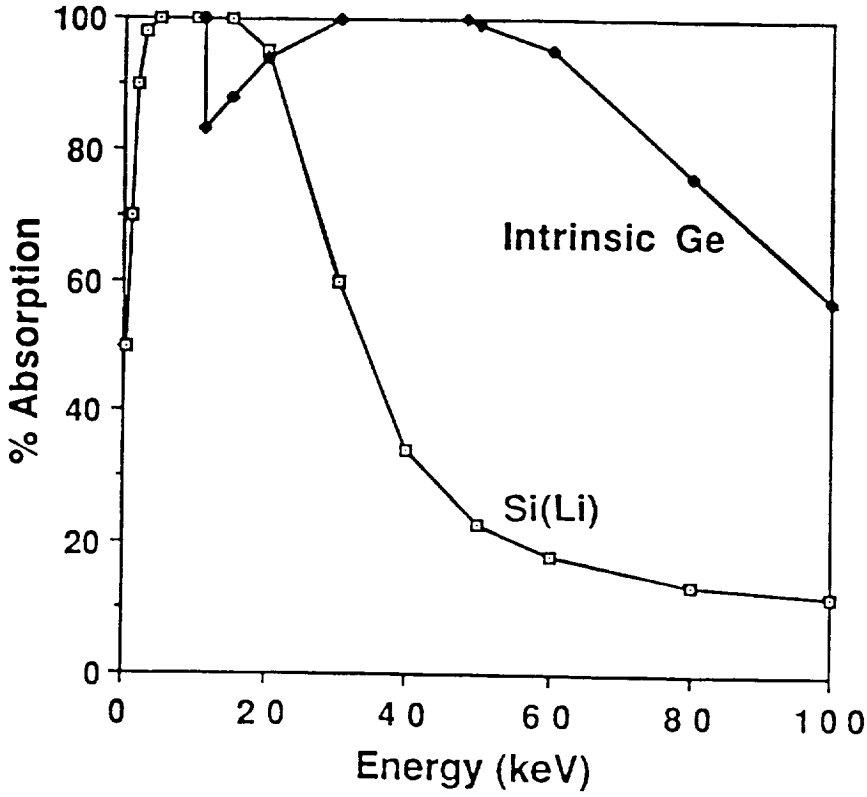

Fig.5. High energy efficiency calculated for Si(Li) and intrinsic Ge detectors. Detector thickness assumed to be 3 mm in both cases [59].

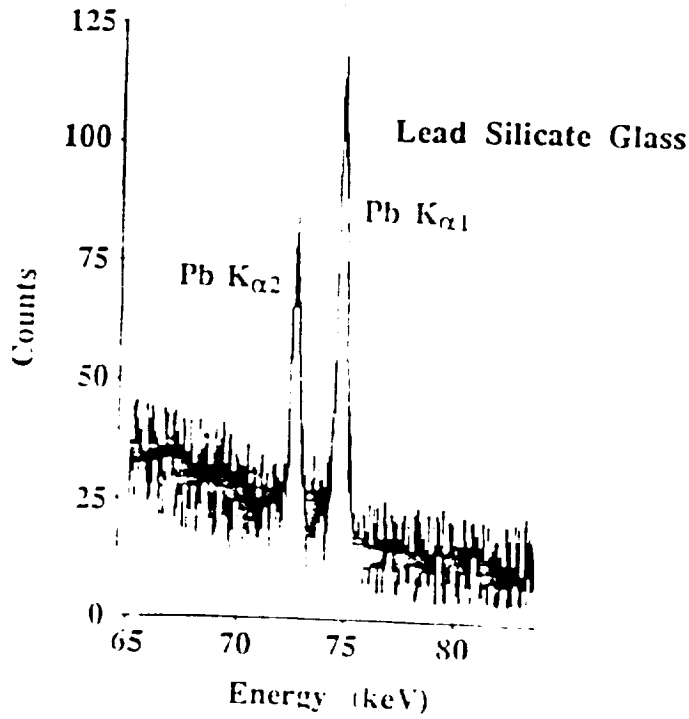

Fig.6. Lead $K_{\alpha 1}$ and $K_{\alpha 2}$ lines from lead silicate glass analyzed in a 200 kV AEM with an intrinsic Ge detector [27] (courtesy San Francisco Press).

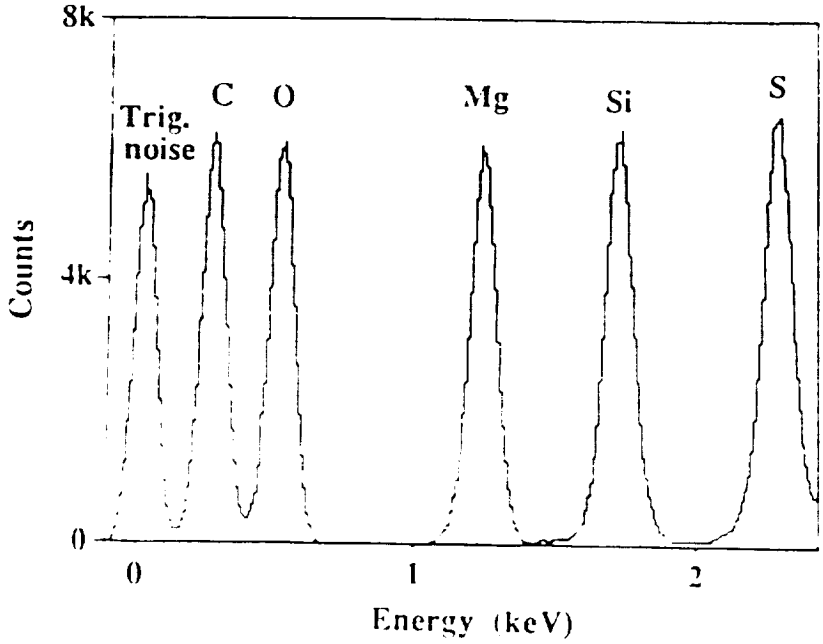

Fig.7. Low energy peaks detected with an intrinsic Ge detector showing a low level of incomplete charge collection [29].

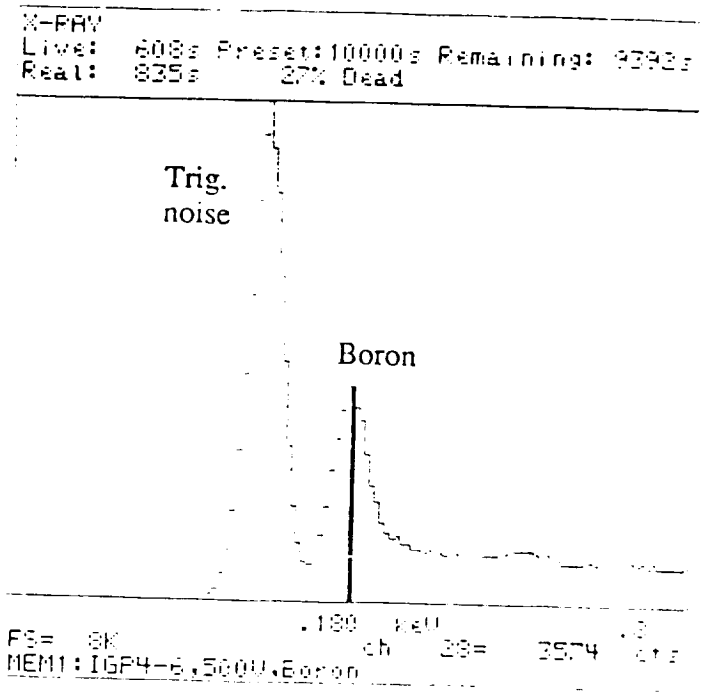

Fig.8. Boron K_α peak collected with an intrinsic Ge detector (courtesy Link Systems).

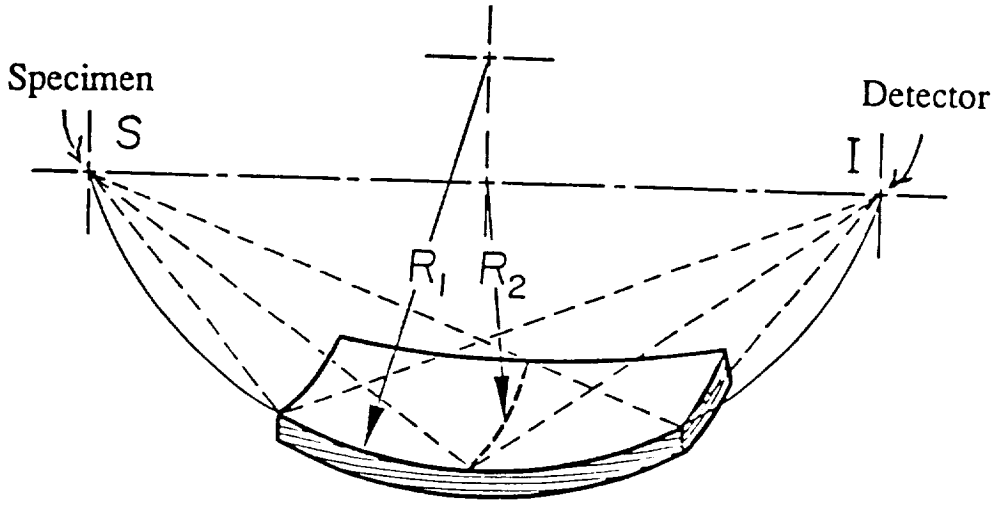

Fig.9. Schematic diagram of a doubly-bent diffracting crystal for a wavelength-dispersive spectrometer [46].